Journal of Hazardous Materials 203–204 (2012) 341–347

Contents lists available at SciVerse ScienceDirect

Journal of Hazardous Materials

journal homepage: www.elsevier.com/locate/jhazmat

Efficient MgO-based mesoporous CO_2 trapper and its performance at high temperature

Kun Kun Han, Yu Zhou, Yuan Chun, Jian Hua Zhu*

Key Laboratory of Mesoscopic Chemistry, School of Chemistry & Chemical Engineering, Nanjing University, Nanjing 210093, China

ARTICLE INFO

Article history:
Received 29 August 2011
Received in revised form
11 December 2011
Accepted 12 December 2011
Available online 19 December 2011

Keywords:
MgO based mesoporous alumina adsorbent
CO_2 capture at high temperature
Flue gas
Environment protection

ABSTRACT

A novel MgO-based porous adsorbent has been synthesized in a facile co-precipitation method for the first time, in order to provide a candidate for trapping CO_2 in flue gas at high temperature. The resulting composite exhibits a mesoporous structure with a wide pore size distribution, due to the even dispersion and distribution of microcrystalline MgO in the framework of alumina to form a concrete-like structure. These sorbents can capture CO_2 at high temperature (150–400 °C), possessing high reactivity and stability in cyclic adsorption–desorption processes, providing competitive candidates to control CO_2 emission.

1. Introduction

Combustion of fossil fuels emits huge amounts of carbon dioxide, contributing to global climate changes [1,2]. Therefore it is necessary to trap CO_2 from flue gas at first, and then sequestrate CO_2 via geological formations, mineralization and ocean storage [3–8]. Various efficient methods have been proposed for CO_2 capture for this purpose, including commercial liquid amine, carbon-based adsorbent and amine-modified mesoporous materials [9–12]. However, most of these methods are carried out at relative low temperature, generally below 100 °C, while the temperature of flue gas vent is usually in the range of 150–400 °C [13,14]. Zeolites and hydrotalcite have been also tested for CO_2 adsorption [15,16], but they are flaccid at high temperatures. Thus, it is crucial to develop new functional material and technique to trap CO_2 from flue gas at high temperature.

Recently, adsorbents based on alkali metal oxide and alkali earth metal oxides with considerable CO_2 uptake and reversibility have been developed [17–19]. Among them Li-based adsorbents is able to trap CO_2; however, decomposition of Li_2CO_3 needs high temperature (800–900 °C) to release CO_2. Moreover, they are expensive [20–22]. Ca-based sorbents can capture CO_2 at 600–700 °C, but temperature above 900 °C is required for their regeneration [23,24].

The relatively high temperature range of the flue gas enables magnesia to be a candidate for CO_2 capture. MgO loaded on Al_2O_3 sorbents can be prepared by impregnation method, and their CO_2 adsorption capacities reach 42 and 60 mg g^{-1} in the absence and presence of water vapor, respectively [25]. Other MgO-based sorbents are prepared by modification of dolomite for CO_2 removal in syngas at high temperature (300–450 °C) and high pressure (20 atm), and their capacity achieves 102–117 mg g^{-1} [26]. Mesoporous silica SBA-15 is treated with sucrose and sulphuric acid to obtain mesoporous carbon (CMK-3) replica through the nano-casting process. With a similar procedure the mesoporous magnesia is then replicated from the mesoporous carbon CMK-3, and it exhibits a maximum CO_2 adsorption capacity of 100 mg g^{-1} at 100 °C [27]. Nevertheless, its application is limited by the complicated preparation and the high cost. Thus, it is necessary to develop new CO_2 trappers with high capacity at high temperature and atmospheric pressure.

Herein, a new MgO-based mesoporous adsorbent is synthesized using a co-precipitation method, which allows both the synthesis and the modification of mesoporous alumina to be performed in one-pot process. As the result, a mass of MgO can be dispersed in the sorbent, resulting in a composite having considerably large surface and pore volume. The new adsorbents are used for CO_2 capture in the temperature range of 150–400 °C under atmospheric pressure. Since the flue gas usually contains 8–17 vol.% of water vapor in the practical condition [24], these MgO-based composites have been also assessed their actual performance of trapping CO_2 in the presence of vapor.

* Corresponding author. Tel.: +86 25 83595848; fax: +86 25 83317761.
E-mail address: jhzhu@netra.nju.edu.cn (J.H. Zhu).

0304-3894/$ – see front matter © 2011 Elsevier B.V. All rights reserved.
doi:10.1016/j.jhazmat.2011.12.036

2. Experimental

In the typical synthesis, 6.38 g P123, poly(ethylene oxide)–poly(propylene oxide)–poly(ethylene oxide) (EO–PO–EO) triblock co-polymers, were dissolved in 20 g H_2O, followed by the addition of $Al(NO_3)_3{\cdot}9H_2O$ (0.05 mole). The resulting mixture was stirred at 40 °C for 24 h to form a clear sol and then aged at 45 °C for 6 h. Thereafter, a solution containing different amount of $Mg(NO_3)_2{\cdot}6H_2O$ and 20 g H_2O was dropwise added under gentle stirring conditions. After the sol was further aged of 6 h, a stoichiometric amount of $NH_3{\cdot}H_2O$ containing 0.2–0.3 mol of OH^- was slowly added under slow stirring, and then the gel was transferred into a teflonlined autoclave for hydrothermal treatment at 100 °C for 24 h. Afterward, it was transferred to a beaker for evaporation at 90 °C. Finally, the solid was calcined at 600 °C for 4 h, converting boehmite to γ-Al_2O_3 while the incorporated $Mg(OH)_2$ was transformed into MgO. The samples were named as 5A*n*M, where 5 and *n* represent the molar quantities of Al and Mg, respectively. For example, 5A5M composite was prepared with 0.05 mol aluminum and 0.05 mol magnesium, while 5A0M meant the absence of magnesium. The mass fraction of MgO incorporated into the sample of 5A3M, 5A5M and 5A7M is 24%, 39% and 55%, respectively. For comparison, MgO was obtained from the calcination of $Mg(NO_3)_2{\cdot}6H_2O$ at 600 °C.

X-ray diffraction (XRD) patterns of sample were recorded using an ARL XTRA diffractometer (power 40 kV, 40 mA) with Cu-Kα radiation in the 2-theta range from 0.5° to 8° or from 6° to 80°. N_2 adsorption–desorption isotherms were measured on a Micromeritics ASAP 2020 system at −196 °C, being the sample outgassed at 300 °C for 4 h prior to test. The Brunauer–Emmett–Teller (BET) method was utilized to calculate the specific surface areas of sample. The pore size distribution was derived from the adsorption branch of the isotherm using the Barrett–Joyner–Halanda (BJH) algorithm, and the total pore volume was estimated from the amount adsorbed at a relative pressure (P/P_0) of 0.99. SEM images and X-ray mapping images of sample were obtained with Hitachi S4800 microscopes at 20 kV, 10 mA and 40 kV, 15 mA, respectively.

To perform the FTIR test of CO_2 adsorbed on sorbent, the self-supporting wafer with the density of 13 mg cm^{-2} was activated at 500 °C for 4 h under vacuum. Afterward the sample was taken the background spectrum at 25 °C, and then contacted with CO_2 at 200 °C for 0.5 h followed by evacuation of 0.5 h, prior to taking the spectrum at 25 °C. Then, the sample was kept with CO_2 at 300 °C, 400 °C, 500 °C for 0.5 h and then recorded at 25 °C by a VERTEX 70 FTIR spectrometer with a resolution of 2 cm^{-1}.

CO_2 adsorption was performed as previously reported [24]. In a typical process, 75 mg of granular sample with a size of 20–40 mesh were heated in a flow of N_2 (dry, 99.995%) at 600 °C for 2 h, then cooled to the given temperature. The simulated flue gas containing CO_2, N_2 with or without H_2O was introduced to contact with the sample for 1 h, and its speed was kept 50 ml min^{-1} (room temperature). Afterward, the sample was purged with a N_2 flow for 10 min followed by the cooling down to room temperature. Temperature programmed desorption (TPD) of CO_2 was performed from room temperature to 600 °C at a rate of 8 °C min^{-1} in the flow of N_2, while the liberated CO_2 was detected by an "online" Varian 3380 gas chromatograph and quantitatively measured by the external standard method. A drying tube of P_2O_5 was used in the reactor outlet to drastically absorb the moisture desorbed from the sample, ensuring the CO_2 to be the sole entering gas into chromatograph. In the cyclic adsorption–desorption tests, the sample was allowed to re-adsorb CO_2 in the same manner aforementioned as soon as the entire desorption process was finished. TG-MS analysis of sample was conducted on a thermobalance (STA-499C, Netzsch) coupled with a mass analyzer (QUADSTAR-422, Pfeiffer). The composite adsorbed CO_2 in the reactor with the feed gas of 10 vol.% CO_2, 10 vol.% H_2O, and 80 vol.% N_2 at 200 °C in the manner aforementioned, and then was transferred for TG-DSC measurement. The CO_2 adsorbed sample was heated from room temperature to 600 °C at a rate of 8 °C min^{-1} and held at 600 °C for 1 h in a continuous flow of Ar (30 mL min^{-1}), and the effluent of desorption was simultaneously analyzed with mass spectrometer.

3. Results and discussion

3.1. Structural characterization of 5AnM composites

Fig. 1A displays low-angle XRD patterns of 5A*n*M samples. One diffraction with 2-theta value of about 1.1° is observed on the pattern, representing the mesoporous structure with no long-range order. As the Mg-content of sample increases, this diffraction peak lowers but not shift, indicating the declined ordered structure. The parent sample 5A0M exhibits typical diffraction lines of γ-Al_2O_3 (JCPDS 10-0425) with 2-theta values of 39.47°, 45.84° and 67.00° (Fig. 1B). Other 5A*n*M composites possess the diffraction peaks of MgO at 2θ of 42.99° and 62.34°, and these peaks become slightly stronger and broader as the amount of incorporated Mg species increases. The (4 0 0) and (4 4 0) diffraction lines of alumina shift to lower diffraction angles after introduction of magnesia, because they are overlapped with the diffraction lines of the guest. As the result, three main diffraction peaks on the pattern of 5A7M can be attributed to that of magnesia (Fig. 1B). Although a lot of MgO is incorporated into the composite such as 5A7M, no sharp and dramatically increased XRD peaks emerge on the pattern, because microcrystalline structure of MgO forms in the framework [29].

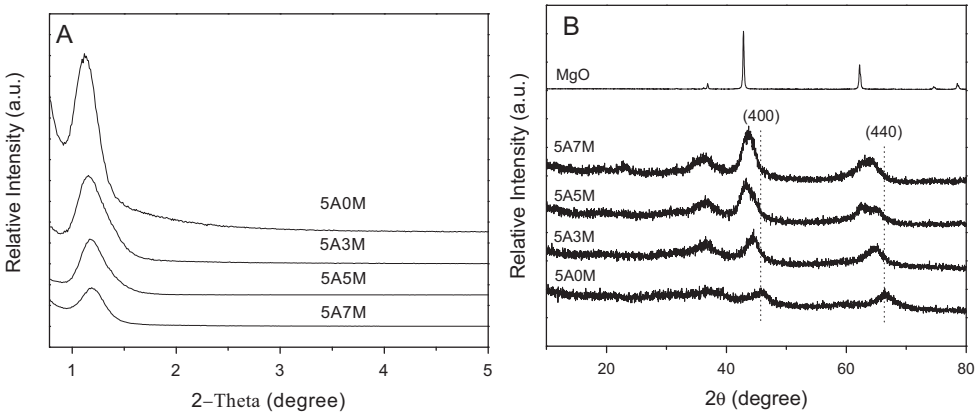

Fig. 1. Low-angle (A) and wide-angle (B) XRD patterns of 5A*n*M sample and MgO.

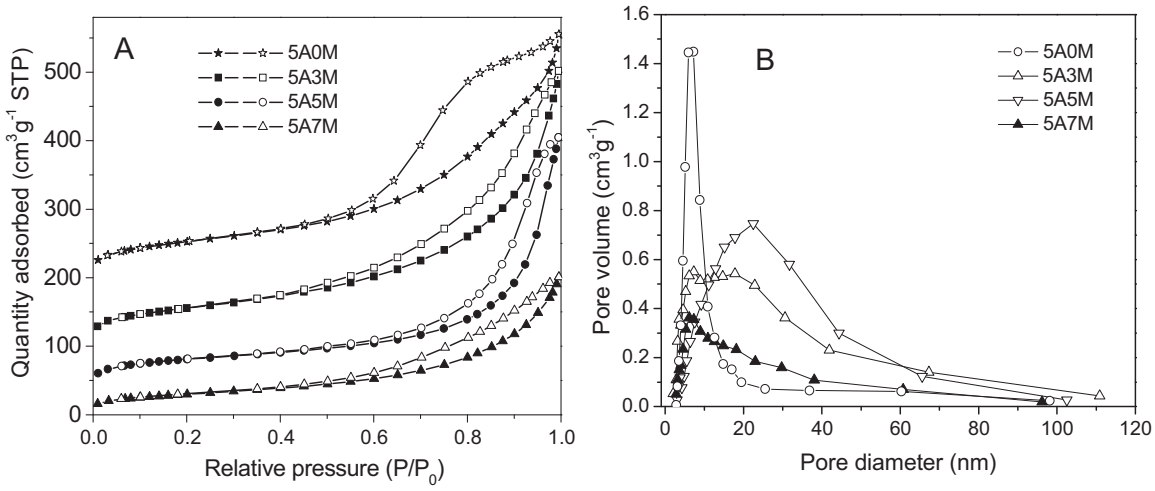

Fig. 2. Nitrogen sorption isotherms (A) and pore size distributions of 5A*n*M samples (B). In nitrogen sorption isotherms (A), closed and open symbols are used to represent the adsorption and desorption isotherms, respectively.

Fig. 2 depicts the N_2 adsorption–desorption isotherms and pore size distributions of 5A*n*M samples. All isotherms are of classical type IV with an obvious hysteresis loop, indicating the mesoporosity of these composites. N_2 uptake emerges at relative pressure of 0.5–0.99 in the isotherms of 5A*n*M samples (Fig. 2A), indicating the formation of mesopore with wide pore sizes (4–80 nm). The hysteresis loops become smaller with the increased Mg-content of samples, implying the declined mesoporous structure. At the same time, the surface area and pore volume are decreased as reported in Table 1. Parent 5A0M has a relatively small average pore diameter of 7 nm, while other 5A*n*M samples have average pore diameter of about 10 nm due to incorporation of magnesia. Mg-containing samples show significant variation of pore size as 5A3M has two sizes (Fig. 2B). These results show that the composite of 5A*n*M has a mesoporous structure with wide pore size distribution. Removing P123 surfactant template and converting boehmite to crystalline γ-Al_2O_3 in calcination procedure can generate the mesostructure with small pores [30]. The introduced Mg species seem to be incorporated into the framework of alumina, reducing the order of framework and lowering pore volume and surface area, while widening the average pore size of the material.

Fig. 3A shows the SEM image of 5A5M sample. It composes of irregular particles with some cumulate pores as shown in the inserted image with high magnification. Figs. 3B and S1 depict the EDX spectrum of 5A5M, 5A3M and 5A7M samples, respectively, showing the presence of Mg and Al. The Mg/Al atomic ratio of the samples is reported in Table 1. Even though several random areas are selected for EDX analysis, the detected Mg/Al molar ratio of 5A3M, 5A5M and 5A7M is 0.64, 0.95 and 1.42, respectively, almost same as that calculated (Table 1). This result suggests a homogeneous distribution of Mg species in these composites. Figs. 3C, D and S2 show the X-ray mapping of 5A3M, 5A5M and 5A7M, in which the microcrystalline MgO and Al_2O_3 seem to be even dispersed in nano level.

Fig. 4 reports the IR spectra of CO_2 adsorbed on 5A5M sample at 200 °C, in which the O—C—O stretching vibration at 1320 cm^{-1} can be attributed to bidentate carbonate and that at 1511 and 1590 cm^{-1} ascribed to unidentate carbonate species [31]. As the sample is evacuated at higher temperature, these peaks gradually decline. Finally bidentate carbonate species disappear after the evacuation at 500 °C while unidentate ones survive but their intensity is dramatically lowered.

3.2. CO_2 trapping by MgO-based porous composite

Table 1 reports the CO_2 adsorption on 5A*n*M samples detected by TPD method. Both parent 5A0M and MgO itself have a weak adsorption capacity of 6 and 9 mg g^{-1} at 200 °C. Incorporation of magnesia allows 5A*n*M samples to trap CO_2 amounts several times higher than their parent in the same conditions. In particular, 5A3M, 5A5M and 5A7M samples adsorbed 45, 77 and 37 mg of CO_2 per gram, respectively. Two factors should be taken into account for the phenomenon: the homogeneous dispersion of MgO in Al_2O_3 framework and the mesopores in the composite, which ensures CO_2 to easily contact with the active sites. Different situation emerges if the adsorption efficiency of sample is calculated by its surface area. MgO is the champion and 5A5M becomes the runner-up. Either 5A3M or 5A7M show the lower efficiency than 5A5M, revealing the property–function relation of magnesia guest. The CO_2 adsorption capacity of sample relates to the amount of adsorption site available [12], which may be a balance of the content of Mg species and their dispersion in the

Table 1
The textural properties and CO_2 adsorption capacities of 5A*n*M samples.

Sample	MgO	5A0M	5A3M	5A5M	5A7M
BET surface area (m^2 g^{-1})	About 10	253	202	177	108
Pore volume (cm^3 g^{-1})	–	0.52	0.48	0.45	0.26
D_p (nm)	–	7.2	10.2	10.3	9.8
Mg/Al atomic ratio calculated	–	0	0.6	1.0	1.4
Detected by EDX method	–	0	0.64	0.95	1.42
CO_2 trapped at 200 °C (mg g^{-1})	9	6	45	77	37
(mg m^{-2}, A)	0.9	0.02	0.22	0.43	0.34
CO_2 trapped at 200 °C with vapor (mg g^{-1})	37	7	93	131	84
(mg m^{-2}, B)	3.7	0.03	0.46	0.74	0.78
B/A	4.1	–	2.09	1.72	2.29

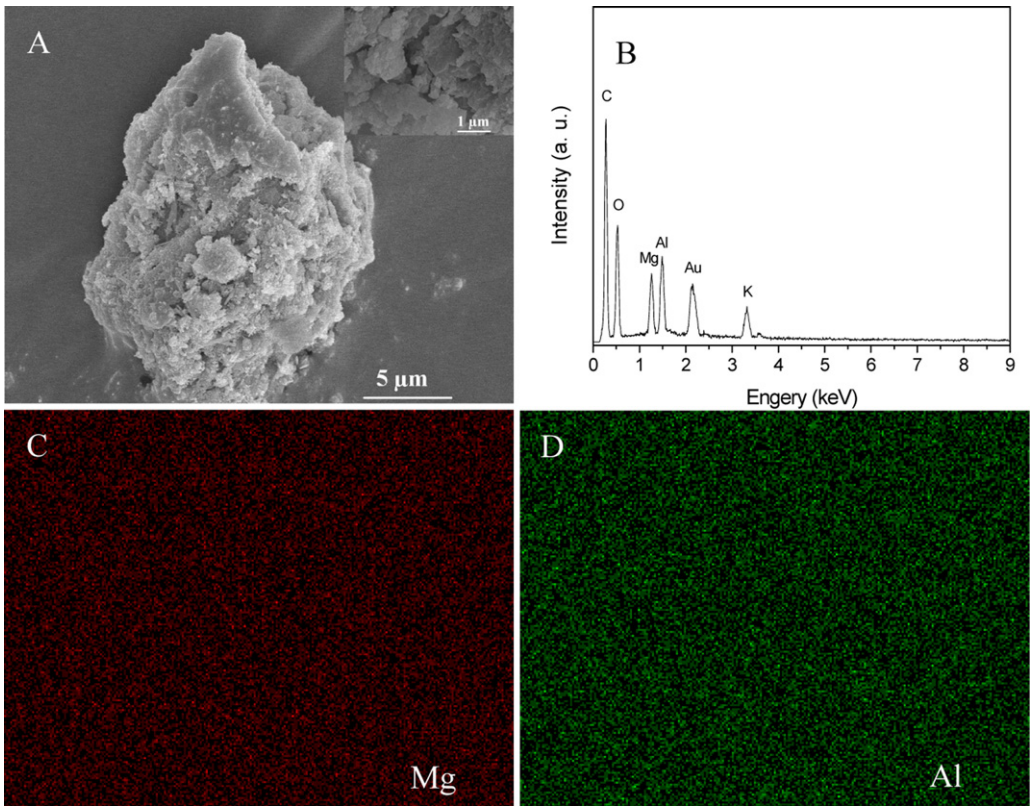

Fig. 3. SEM images (A), EDX spectrum (B), and X-ray mapping (C, D) of 5A5M sample, in which the magnification is 5,00,000.

surface of samples. Since 5A5M composite exhibits the highest adsorption performance, it is selected for further investigations.

Fig. 5A displays the TPD profile of CO_2 from 5A5M samples in the absence or presence of water vapor. Two desorption peaks are observed at 211 °C and 463 °C in the case of adsorbing CO_2 at 200 °C, and they can be tentatively assigned to two kinds of adsorption sites at 200 °C [25]. Once the water vapor is introduced in adsorption procedure, the climax of desorption peaks shift to higher temperature, 333 °C and 524 °C, while the amount of desorption is obviously increased. Similar phenomena also emerge on 5A3M and 5A7M, but absent on parent 5A0M sample (Table 1). The amount of CO_2 desorbed from 5A3M, 5A5M and 5A7M is enlarged about 110%, 70% and 130% (Figs. 5B and S3), respectively. However, almost all of the trapped CO_2 can be desorbed from the sample at 600 °C (Fig. 5A), which will facilitate the regeneration and cycle utilization of the CO_2-trapper. The function of vapor to enhance the capability of MgO-based composite in trapping CO_2 at 200 °C may involve the mechanism. The main reaction between CO_2 and MgO at high temperature without vapor is the formation of carbonate as described: $MgO + CO_2 = MgCO_3$ [29]. With the introduction of water vapor, a transient $Mg(OH)_2$ component is distinctly formed when the MgO is exposed to the steam environment [32], and then the capture process of CO_2 involves the reactions: $MgO + H_2O = Mg(OH)_2$, $Mg(OH)_2 + CO_2 = MgCO_3 + H_2O$. It is suggested that the kinetics of CO_2 capture by $Mg(OH)_2$ is much faster than MgO [33]. Therefore, 5A*n*M adsorbents can capture more CO_2 from feed gas. Apparently, this feature of 5A*n*M composites is beneficial for their potential application for capturing CO_2 under practical conditions, because flue gas contains water vapor [24].

Fig. 6 illustrates the TG-DSC and MS analysis on the CO_2 desorbed from 5A5M sample. The sample losses about 2% of weight at 300 °C, and an endothermic peak appears on the DSC spectrum. Upon heating the sample from 300 °C to 600 °C, the TG curve dramatically declines to indicate the further weight loss of about 10% meanwhile a high endothermic peak emerges (Fig. 6A), mirroring the occurrence of desorption in this temperature range. CO_2 desorption is also confirmed by MS analysis (Fig. 6B), in which a large desorption of CO_2 is detected from 200 °C to 600 °C.

Fig. 7A examines the effect of adsorption temperature on the amount of CO_2 captured by 5A5M. The interaction of CO_2 with the MgO-based sample in the presence of vapor is an exothermic process, according to the DSC curve in Fig. 6A. And referring to literature [33] the reaction is $MgO\ (s) + H_2O\ (g) = Mg(OH)_2\ (s)$ $\Delta H = -81.48\ kJ\ mol^{-1}$, $Mg(OH)_2\ (s) + CO_2\ (g) = MgCO_3(s) + H_2O\ (g)$, $\Delta H = -19.66\ kJ\ mol^{-1}$, therefore this composite should exhibit

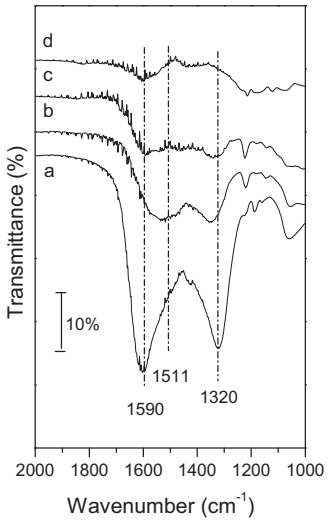

Fig. 4. FTIR difference spectra of CO_2 adsorbed on 5A5M sample at (a) 200 °C, (b) 300 °C, (c) 400 °C, and (d) 500 °C.

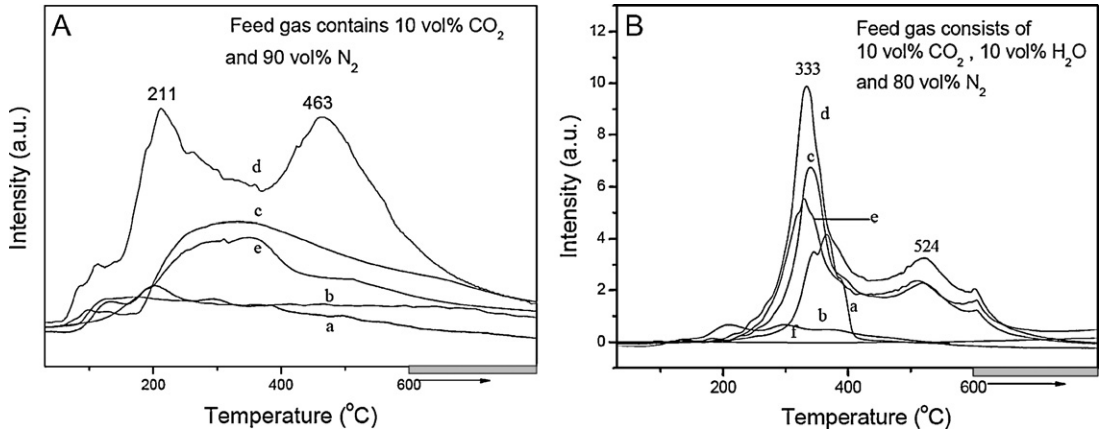

Fig. 5. CO_2-TPD profiles of samples in the absence (A) or presence (B) of vapor, (a) MgO, (b) 5A0M, (c) 5A3M, (d) 5A5M, (e) 5A7M, and (f) blank curve.

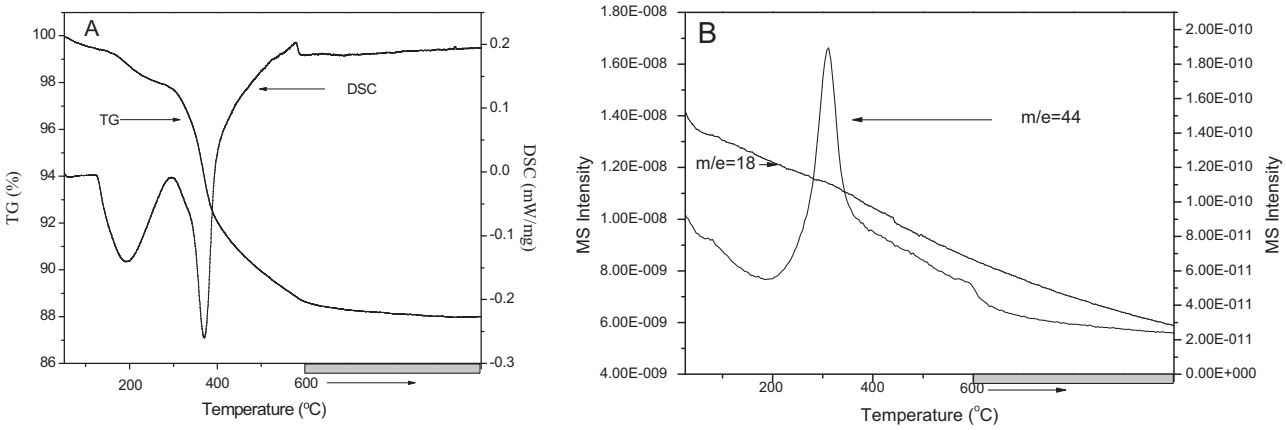

Fig. 6. TG-DSC (A) and MS (B) curves of CO_2 desorption from 5A5M sample.

a higher activity at relatively low temperature. However, the CO_2 trapping capacity by 5A5M sample is 117 mg g^{-1} at 150 °C, lower than that at 200 °C (131 mg g^{-1}). At higher temperature the adsorption capacity decreases to 100 mg g^{-1} at 300 °C and 41 mg g^{-1} at 400 °C (Figs. 7A and S3). The interaction of CO_2 with 5A5M sample may be kinetically controlled at relatively low temperature hence the reactivity of the composite is slightly enhanced at 200 °C in comparison with that at 150 °C. Nonetheless, the rate of reverse reaction is increased at a higher temperature so that the thermodynamics becomes dominant, leading to lower CO_2 adsorption capacities. Fig. 7B shows the cyclical capacity of 5A5M in the trapping-desorption of CO_2 at 200 °C with the presence of vapor. This sample exhibits a high CO_2 trapping capacity of 115 mg g^{-1} in the 6th cycle, equaling to 88% of that in 1st cycle (131 mg g^{-1}). For practical use, the CO_2 trapper should not only possess a high capability, but also display a stable cyclic utilization performance. The high activity and stability of 5A5M composite in the trapping of CO_2 at 200 °C are beneficial for its potential practical applications.

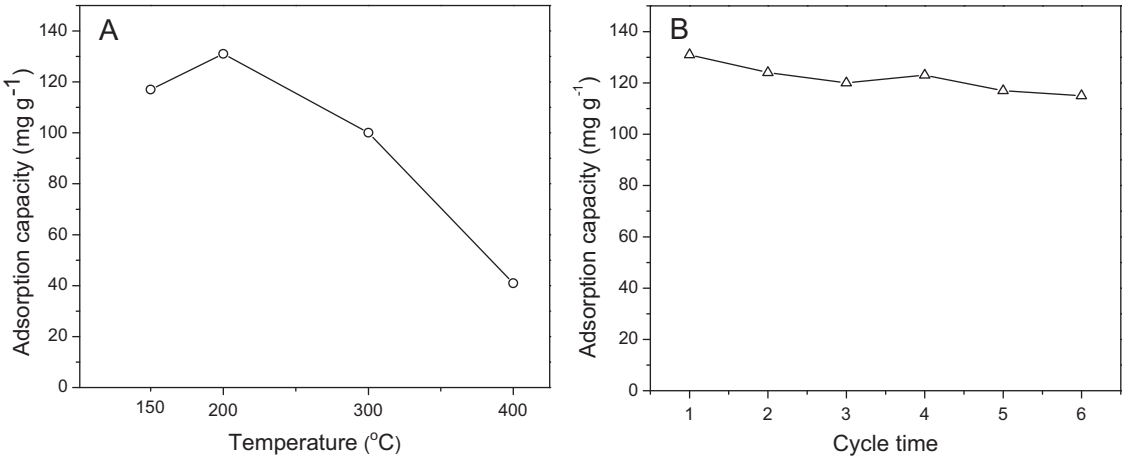

Fig. 7. CO_2-trapping (A) and the cycle utilization at 200 °C (B) of 5A5M sample.

4. Discussion

Fabrication of favorable structure/texture is crucial for the MgO based mesoporous composite to trap CO_2 at 200 °C. The capturer should have enough active sites with optimal accessibility to contact with CO_2, and then desorb CO_2 at a higher temperature. Therefore, the candidate needs to have a pore structure with a good flexibility to bear the structural variation in adsorption/reaction and desorption/regeneration. Moreover, the active component magnesia should be highly dispersed and felicitously separated in such porous structure in order to tolerate the cycle of formation and decomposition of carbonate.

Alumina and magnesia are chosen to fabricate the CO_2 capturer. Alumina fails to trap CO_2 at 200 °C (Table 1), but it can form the necessary mesoporous carrier, unlike silica that reacts with magnesium at high temperature to form the weak basic compounds [34]. Magnesia cannot assemble to mesoporous adsorbent in common hydrothermal synthesis, and MgO itself exhibits a poor capacity of trapping CO_2 (9 mg g^{-1}, Table 1) due to its small surface area. Consequently, we plan to disperse magnesia on the support of alumina in order to form desirable composite.

In our synthesis, aluminate reactant was allowed to contact with surfactant at first, in order to let Al species interact with P123 micelles through the hydrogen bonding between the surfactant and the nitrate anions [34]. And then magnesium salt incorporates inside the aggregation of host through co-precipitation. During the evaporation step in the synthesis cations may undergo complexation with the hydrophilic EO groups in P123 upon the evaporation of water [34], and these interactions among PEO-Mn^+-anion promote the dispersion level of guest oxide species in the carrier, probably through insertion and/or micro-crystallization. Judged from the XRD pattern of 5A*n*M samples (Fig. 1), formation of hydrotalcite is excluded, and the MgO is not simply coated on the mesoporous alumina. Otherwise, as the Mg-content of sample increased from 24% (5A3M) to 55% (5A7M), the XRD pattern of MgO phase would be drastically strengthened, as that previously reported [28,35]. Rather, based on the results of XRD and X-ray mapping, it seems that magnesia has been inserted into the framework of alumina, probably through micro-crystalline form, resembling that of concrete, in which the magnesia micro-crystals equably insert into the framework formed by alumina. Due to the even insertion of guest into the host framework, there is no surface enriching of MgO but the unique distribution of Mg and Al (Table 1). The surface Al/Mg molar ratio of composite determined by X-ray mapping method is close to that calculated. However, this insertion affects the pore structure of resulting composite, the pore size distribution is widened and the most probably pore size is enlarged (Fig. 2). As the Mg-content of composite increases, its pore structure is distorted and it seems to be non-ordered. Fortunately, it still owns a considerably high capability of capture CO_2 and the stability in recycle use at 200 °C (Figs. 5 and 7), thanks to the high dispersion of magnesia in alumina support.

Magnesia guests are accumulated to be micro-crystals in the composite, and only the ones on the top contact with CO_2. Thus, the property–function relation of magnesia in 5A*n*M composites is assessed by the efficiency of per square meter surface area. Mesoporous alumina has a very weak ability, and this data increases as magnesia is incorporated (Table 1), achieving the maximum at 5A5M sample (0.43 mg m^{-2}). Considering the surface consisting of equal molar magnesia and alumina, this value is close to that of MgO itself in the adsorption of CO_2 at 200 °C in dry gas stream: since the magnesia was diluted with equal mole of alumina in this composite where equal molar alumina exist in MgO with an even dispersion, and alumina has a very low adsorption efficiency of CO_2 (0.02 mg m^{-2}), the mean adsorption value of MgO in the composite should divide 2 to be equal to 0.45 mg m^{-2} (0.9/2 = 0.45 mg m^{-2}). Presence of vapor promotes the activity of 5A*n*M composite in trapping of CO_2 at 200 °C (Figs. 5 and S3), through the formation of $Mg(OH)_2$ that can fast react with CO_2 [32]. Moreover, the difference among the efficiency of three 5A*n*M samples (Table 1) is decreased, among them 5A7M exhibits the highest promotion. On the other hand, the efficiency of MgO in trapping CO_2 at 200 °C with vapor is much higher than that of 5A5M (about 5 times, Table 1), which implies the different property–function relation between them. If we can optimize the distribution of magnesia guest in porous support, it is hopeful to enhance the performance of trapping CO_2 at high temperature.

5. Conclusion

Some conclusive remarks can be tentatively derived from the results mentioned above.

(1) A new MgO-based mesoporous composite has been successfully synthesized by an one-pot synthesis strategy.
(2) With the microcrystalline MgO existed in the framework of alumina, this composite can capture amounts of CO_2 of 77 and 131 mg g^{-1} at 200 °C in the absence or presence of water vapor, respectively.
(3) This CO_2-trapper can be regenerable at 600 °C, being stable for cyclic adsorption.

Acknowledgments

Financial support from NSFC (20873059 and 21173117), MSTC (2008AA06Z327) and Analysis Center of Nanjing University is gratefully acknowledged.

Appendix A. Supplementary data

Supplementary data associated with this article can be found, in the online version, at doi:10.1016/j.jhazmat.2011.12.036.

References

[1] J.M. Melillo, A.D. McGuire, D.W. Kicklighter, B. Moore, C.J. Vorosmarty, A.L. Schloss, Global climate change and terrestrial net primary production, Nature 363 (1993) 234–240.
[2] C.S. Song, Global challenges and strategies for control, conversion and utilization of CO_2 for sustainable development involving energy, catalysis, adsorption and chemical processing, Catal. Today 115 (2006) 2–32.
[3] H. Herzog, What future for carbon capture and sequestration, Environ. Sci. Technol. 35 (2001) 148–153.
[4] S. Bachu, CO_2 storage in geological media: role, means, status, and barriers to deployment, Prog. Energy Combust. Sci. 34 (2008) 254–273.
[5] V. Ferrini, C. De Vito, S. Mignardi, Synthesis of nesquehonite by reaction of gaseous CO_2 with $MgCl_2$ solution: its potential role in the sequestration of carbon dioxide, J. Hazard. Mater. 168 (2009) 832–837.
[6] L. Zhao, L.Q. Sang, J. Chen, J.F. Ji, H.H. Teng, Aqueous carbonation of natural brucite: relevance to CO_2 sequestration, Environ. Sci. Technol. 44 (2010) 406–411.
[7] S. Mignardi, C. De Vito, V. Ferrini, R.F. Martin, The efficiency of CO_2 sequestration via carbonate mineralization with simulated wastewaters of high salinity, J. Hazard. Mater. 191 (2011) 49–55.
[8] R. Zevenhoven, J. Fagerlund, J.K. Songok, CO_2 mineral sequestration: developments toward large-scale application, Greenhouse Gas Sci. Technol. 1 (2011) 48–57.
[9] S.A. Freeman, J. Davis, G.T. Rochelle, Degradation of aqueous piperazine in carbon dioxide capture, Int. J. Greenhouse Gas Control 4 (2007) 756–761.
[10] U.E. Aronu, H.F. Svendsen, K.A. Hoff, Investigation of amine amino acid salts for carbon dioxide absorption, Int. J. Greenhouse Gas Control 4 (2010) 771–775.
[11] M.L. Gray, Y. Soong, K.J. Champagne, J. Baltrus, R.W. Stevens, P. Toochinda, S.S.C. Chuang, CO_2 capture by amine-enriched fly ash carbon sorbents, Sep. Purif. Technol. 35 (2004) 31–36.
[12] M.B. Yue, L.B. Sun, Y. Cao, Y. Wang, Z.J. Wang, J.H. Zhu, Efficient CO_2 capturer derived from as-synthesized MCM-41 modified with amine, Chem. Eur. J. 14 (2008) 3442–3451.
[13] Y. Zhao, Y.H. Han, T.Z. Ma, T.X. Guo, Simultaneous desulfurization and gas denitrification from flue by ferrate(VI), Environ. Sci. Technol. 45 (2011) 4060–4065.

[14] X.S. Yin, S.P. Li, Q.H. Zhang, J.G. Yu, Synthesis and CO_2 adsorption characteristics of lithium zirconates with high lithia content, J. Am. Ceram. Soc. 93 (2010) 2837–2842.
[15] R.V. Siriwardane, M.S. Shen, E.P. Fisher, J. Losch, Adsorption of CO_2 on zeolites at moderate temperatures, Energy Fuels 19 (2005) 1153–1159.
[16] H.Th.J. Reijers, S.E.A. Valster-Schiermeier, P.D. Cobden, R.W. van den Brink, Hydrotalcite as CO_2 sorbent for sorption-enhanced steam reforming of methane, Ind. Eng. Chem. Res. 45 (2006) 2522–2530.
[17] P.C. Lin, C.W. Huang, C.T. Hsiao, H. Teng, Magnesium hydroxide extracted from a magnesium-rich mineral for CO_2 sequestration in a gas–solid system, Environ. Sci. Technol. 42 (2008) 2748–2752.
[18] S.C. Lee, H.J. Chae, S.J. Lee, B.Y. Choi, C.K. Yi, J.B. Lee, C.K. Ryu, J.C. Kim, Development of regenerable MgO-based sorbent promoted with K_2CO_3 for CO_2 capture at low temperatures, Environ. Sci. Technol. 42 (2008) 2736–2741.
[19] A. Zukal, J. Mayerova, J. Cejka, Alkali metal cation doped Al-SBA-15 for carbon dioxide adsorption, Phys. Chem. Chem. Phys. 12 (2010) 5240–5247.
[20] X.S. Yin, Q.H. Zhang, J.G. Yu, Three-step calcination synthesis of high-purity Li_8ZrO_6 with CO_2 absorption properties, Inorg. Chem. 50 (2011) 2844–2850.
[21] K. Wang, X. Guo, P.F. Zhao, F.Z. Wang, C.G. Zheng, High temperature capture of CO_2 on lithium-based sorbents from rice husk ash, J. Hazard. Mater. 189 (2011) 301–307.
[22] J.C. Abanades, E.S. Rubin, E.J. Anthony, Sorbent cost and performance in CO_2 capture systems, Ind. Eng. Chem. Res. 43 (2004) 3462–3466.
[23] H. Gupta, L.S. Fan, Carbonation–calcination cycle using high reactivity calcium oxide for carbon dioxide separation from flue gas, Ind. Eng. Chem. Res. 41 (2002) 4035–4042.
[24] B.B. Sakadjian, M.V. Iyer, H. Gupta, L.S. Fan, Kinetics and structural characterization of calcium-based sorbents calcined under subatmospheric conditions for the high-temperature CO_2 capture process, Ind. Eng. Chem. Res. 46 (2007) 35–42.
[25] L. Li, X. Wen, X. Fu, F. Wang, N. Zhao, F.K. Xiao, W. Wei, Y.H. Sun, MgO/Al_2O_3 sorbent for CO_2 capture, Energy Fuels 24 (2010) 5773–5780.
[26] A. Hassanzadeh, J. Abbasian, Regenerable MgO-based sorbents for high-temperature CO_2 removal from syngas. 1. Sorbent development, evaluation, and reaction modeling, Fuel 89 (2010) 1287–1297.
[27] M. Bhagiyalakshmi, J.Y. Lee, H.T. Jang, Synthesis of mesoporous magnesium oxide: its application to CO_2 chemisorption, Int. J. Greenhouse Gas Control 4 (2010) 51–56.
[28] M.B. Yue, Y. Chun, Y. Cao, X. Dong, J.H. Zhu, CO_2 capture by as-prepared SBA-15 with an occluded organic template, Adv. Funct. Mater. 16 (2006) 1717–1722.
[29] L.B. Sun, W.H. Tian, X.Q. Liu, Magnesia-incorporated mesoporous alumina with crystalline frameworks: a solid strong base derived from direct synthesis, J. Phys. Chem. C 113 (2009) 19172–19178.
[30] L.B. Sun, J. Yang, J.H. Kou, F.N. Gu, Y. Chun, Y. Wang, J.H. Zhu, Z.G. Zou, One-pot synthesis of potassium-functionalized mesoporous-alumina: a solid superbase, Angew. Chem. Int. Ed. (47) (2008) 3418–3421.
[31] R. Philipp, K. Fujimoto, FTIR spectroscopic study of CO_2 adsorption–desorption on MgO/CaO catalysts, J. Phys. Chem. 96 (1992) 9035–9038.
[32] M. Bhagiyalakshmi, P. Hemalatha, M. Ganesh, P.M. Mei, H.T. Jang, A direct synthesis of mesoporous carbon supported MgO sorbent for CO_2 capture, Fuel 90 (2011) 1662–1667.
[33] D. Wolf, M. Barre-Chassonnery, M. Hohenberger, A. van Veen, M. Baerns, Kinetic study of the water–gas shift reaction and its role in the conversion of methane to syngas over a Pt/MgO catalyst, Catal. Today 40 (1998) 147–156.
[34] Y.M. Wang, Z.Y. Wu, Y.L. Wei, J.H. Zhu, In situ coating metal oxide on SBA-15 in one-pot synthesis, Microporous Mesoporous Mater. (84) (2005) 127–136.
[35] Y.L. Wei, Y.M. Wang, J.H. Zhu, Z.Y. Wu, In situ coating of SBA-15 with MgO: direct synthesis of mesoporous solid bases from strong acidic systems, Adv. Mater. (15) (2003) 1943–1945.